

# Site Amplification in the San Fernando Valley, California: Variability of Site-Effect Estimation Using the *S*-Wave, Coda, and *H/V* Methods

by Luis Fabián Bonilla, Jamison H. Steidl, Grant T. Lindley,  
Alexei G. Tumarkin, and Ralph J. Archuleta

**Abstract** During the months that followed the 17 January 1994 *M* 6.7 Northridge, California, earthquake, portable digital seismic stations were deployed in the San Fernando basin to record aftershock data and estimate site-amplification factors. This study analyzes data, recorded on 31 three-component stations, from 38 aftershocks ranging from *M* 3.0 to *M* 5.1, and depths from 0.2 to 19 km. Site responses from the 31 stations are estimated from coda waves, *S* waves, and ratios of horizontal to vertical (*H/V*) recordings. For the coda and the *S* waves, site response is estimated using both direct spectral ratios and a generalized inversion scheme. Results from the inversions indicate that the effect of  $Q_s$  can be significant, especially at high frequencies. Site amplifications estimated from the coda of the vertical and horizontal components can be significantly different from each other, depending on the choice of the reference site. The difference is reduced when an average of six rock sites is used as a reference site. In addition, when using this multi-reference site, the coda amplification from rock sites is usually within a factor of 2 of the amplification determined from the direct spectral ratios and the inversion of the *S* waves. However, for nonrock sites, the coda amplification can be larger by a factor of 2 or more when compared with the amplification estimated from the direct spectral ratios and the inversion of the *S* waves. The *H/V* method for estimating site response is found to extract the same predominant peaks as the direct spectral ratio and the inversion methods. The amplifications determined from the *H/V* method are, however, different from the amplifications determined from the other methods. Finally, the stations were grouped into classes based on two different classifications, general geology and a more detailed classification using a quaternary geology map for the Los Angeles and San Fernando areas. Average site-response estimates using the site characterization based on the detailed geology show better correlation between amplification and surface geology than the general geology classification.

## Introduction

The study of the effects of local site conditions is one of the most important goals of earthquake engineering. General seismic hazard evaluations are calculated over broad geographical areas; however, as more ground-motion data are collected, the local geologic site condition is emerging as one of the dominant factors controlling the variation in ground motion and determination of the site-specific seismic hazard. Damage to property and loss of life in earthquakes are frequently a direct result of the local site geological conditions affecting the incident ground motion. Consequently, any attempt of seismic zonation must take into account the local site conditions. At present, however, the method by which site amplification is determined is still under investigation among seismologists and earthquake engineers.

It has long been known that each soil type responds differently when it is subjected to ground motion from earthquakes. These observations are made by comparing earthquake records taken from sites with different underlying soil types. Aki (1993) summarizes the results obtained both in Japan and in the United States, showing that the site amplification depends on the frequency of the ground motion and that younger softer soils generally amplify the ground motion relative to older and more competent soils or bedrock. Probably the most outstanding example of site amplification related to local geology was observed during the *M*<sub>s</sub> 8.1 Michoacan earthquake in Mexico in 1985. This event amplified the ground motion by a factor of about 50 for the frequencies between 0.25 and 0.7 Hz (Singh and Ordaz, 1993). This

large value of amplification was observed on soft lake sediments underlying Mexico City and is caused by the strong impedance contrast between the sediments and the bedrock.

Due to the concern about structures built over a great variety of geological sites, it is important to measure the site amplification of ground motion throughout metropolitan regions in earthquake-prone areas. The most frequent empirical technique used for site-response estimation has been the spectral ratio method (Borcherdt, 1970; Borcherdt and Gibbs, 1976). This approach considers the ratio between the spectrum at a site of interest and the spectrum at a reference site, which is usually a nearby rock site. Commonly, coda-wave ratios are used to predict the amplification (Phillips and Aki, 1986; Chin and Aki, 1991; Mayeda *et al.*, 1991; Fehler *et al.*, 1992; Koyanagi *et al.*, 1992; Kato *et al.*, 1995; Su and Aki, 1995; Su *et al.*, 1996). The coda-wave method is popular with researchers due to the abundance of data provided by microearthquake observation networks and because the coda spectrum can be separated into source, site, and path effects. Conversely, recordings of the direct *S* waves often consist of a more limited data set, because the microearthquake observation networks can be saturated during the strongest part of the ground motion. In addition, many of the stations in these networks consist of only a single-component high-gain vertical sensor, which is not optimally oriented to record direct *S* waves. However, during recent years, with more instrumentation and new events, seismologists have been studying the spectral ratio using *S* waves (Hartzell, 1992; Field *et al.*, 1992; Steidl, 1993; Field and Jacob, 1995; Margheriti *et al.*, 1994; Gao *et al.*, 1996; Kato *et al.*, 1995; Hartzell *et al.*, 1996; Su *et al.*, 1996; Field, 1996).

The spectral ratio method, however, depends on the availability of an adequate reference site (one with negligible site response). Such a site may not always be available, and alternate techniques called nonreference site methods have been applied to site response studies in these cases. One of these methods to estimate site response uses the spectral ratio between the horizontal and vertical (*H/V*) spectra of the *S*-wave window for each site (Lermo and Chávez-García, 1993). This method is based on the so-called receiver-function technique applied to studies of the upper mantle and crust using teleseismic records (e.g., Langston, 1979), which assumes that the local site conditions are relatively transparent to the motion that appears on the vertical component.

In spite of this large number of studies, seismologists are still debating which method gives better results. Recently, Margheriti *et al.* (1994), Steidl *et al.* (1995), and Field (1996) have found that the coda method differs from the direct *S*-wave spectral ratio. Studies of the *H/V* method (e.g., Lachet and Bard, 1994; Lachet *et al.*, 1996; Field and Jacob, 1995; Field, 1996) show that estimates of the frequency of the predominant peak are similar to that obtained with traditional spectral ratios; however, the absolute level of site amplification does not correlate with the amplification obtained from the more traditional methods.

In this article, the coda, *S*-wave, and *H/V* methods are compared. For the coda and *S*-wave methods, a generalized inversion scheme is also compared with direct spectral ratios. In order to evaluate the differences between the methods, the uncertainties of each method are estimated.

## Data

Immediately following the 17 January 1994 Northridge earthquake, seismologists in coordination with the Southern California Earthquake Center (SCEC) responded by deploying portable stations in the epicentral area and throughout the metropolitan Los Angeles region. The participants in this collaborative effort included The California Institute of Technology (Caltech), Kinemetrics Inc., Lawrence Livermore National Laboratories (LLNL), San Diego State University (SDSU), The United States Geological Survey (USGS), the University of California at San Diego (UCSD), the University of California at Santa Barbara (UCSB), and the University of Southern California (USC). More than 100 portable instruments were maintained in this region within 7 weeks following the mainshock. The instruments consisted of both short-period and broadband velocity sensors, along with strong-motion accelerometers recording on either 12-, 16-, or 24-bit dataloggers (Edelman and Vernon, 1995).

In this study, 38 records from aftershocks of the Northridge earthquake were analyzed. Figure 1 shows the location of the events as well as the stations used. Table 1 lists the hypocentral parameters of the events, and Table 2 shows the coordinates of the stations used, their instrument characteristics, and the geology of each site. All of these aftershocks present the best solution (A class in the SCSN catalog) in their hypocentral location and have magnitudes from 3.0 up to 5.1 and focal depths between 0.2 and 19.0 km. Thirty-one stations, with six data channels each, were used to estimate the site amplification in the San Fernando Valley and the surrounding mountains. Table 3 shows the matrix of events and recording stations used in this study.

The stations in this study were composed primarily of the SCEC portable deployment, with a few TERRAscope, and Southern California Seismic Network Stations (SCSN). All the velocity sensors were three components consisting of L4-C (1.0-Hz natural frequency), L22 (2.0-Hz natural frequency), CMG3T (0.033-Hz natural frequency), STS2 (0.008-Hz natural frequency), and STS1 (0.004-Hz natural frequency) sensors. The accelerometers were three-component FBA23 (flat response between 0 and 50 Hz) and CMG5 (flat response between 0 and 100 Hz) sensors (Edelman and Vernon, 1995; Wald *et al.*, 1995). Because of this variety of instruments, the instrument response was removed from all the recordings, and the velocity channels were highpass filtered with a cutoff frequency of 0.5 Hz. In addition, all the signals were visually inspected, and those with too much noise and other problems were discarded.

Figure 2a shows an example of acceleration time histories for the event 3147406 on 29 January,  $M = 5.1$ . The

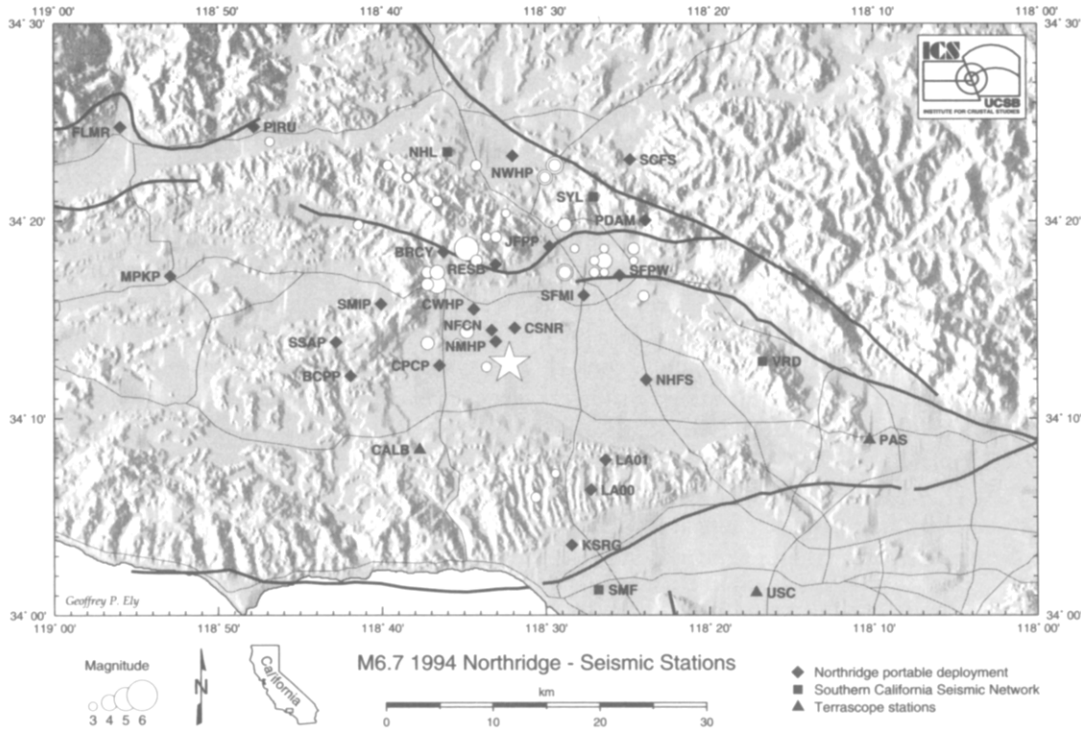


Figure 1. Regional map showing the epicenters (circles) and recording sites (Portable deployment, solid diamonds; SCSN, solid squares; and TERRAscope stations, solid triangles) used in this study. Shaded topography, faults (thick lines), and highways (thin lines) are also shown. Northridge mainshock epicenter shown by large star.

acceleration values at each station have been multiplied by its corresponding  $S$ - $P$  time. However, it is remarkable that before the multiplication, the acceleration at station BRCY is 0.8, 0.7, and 0.45  $g$  on the two horizontals and vertical components, respectively. Many other stations recorded over 0.2  $g$  for this event. Figure 2b shows an example of velocity time histories and the chosen lapse time for the coda window for the event 3147539 on 29 January,  $M = 3.4$ .

## Methods

### Site Amplification from $S$ Waves

**Direct Spectral Ratios.** A seismogram may be represented as the convolution of the source, path, site effect, and instrument response:

$$A_{ij}(f) = S_i(f)P_{ij}(f)G_j(f)I_j(f), \quad (1)$$

where  $S_i(f)$  is the source term of the  $i$ th event,  $P_{ij}(f)$  is the path term between the  $i$ th event and the  $j$ th station,  $G_j(f)$  is the site term for the  $j$ th station, and  $I_j(f)$  is the instrument-response term for the  $j$ th station. After removing the instrument response for each station, the spectral ratio is obtained by dividing the Fourier spectrum of the acceleration for the  $S$  wave at the  $j$ th station by the spectrum of the  $S$  wave at the  $k$ th reference station:

$$\frac{A_{ij}(f)}{A_{ik}(f)} = \frac{S_i(f)P_{ij}(f)G_j(f)}{S_i(f)P_{ik}(f)G_k(f)}. \quad (2)$$

The source term is not necessarily the same for the  $j$ th and  $k$ th stations because of focal mechanism and directivity effects. However, by using a large enough number of events, these effects are expected to be averaged out. Thus, equation (2) can be rewritten as

$$\frac{A_{ij}(f)}{A_{ik}(f)} = \frac{G_j(f)P_{ij}(f)}{G_k(f)P_{ik}(f)}. \quad (3)$$

If the separation between the  $j$ th and  $k$ th stations is less than their hypocentral distances, it is a reasonable assumption that the path terms for both stations are the same. The spectra of the data were corrected for geometrical spreading by multiplying each spectrum at the  $j$ th station for the  $i$ th event by its corresponding  $S$ - $P$  time and assuming that the effect of  $Q_s$  is negligible. Thus, equation (3) becomes

$$\frac{A_{ij}(f)}{A_{ik}(f)} = \frac{G_j(f)T_{ij}}{G_k(f)T_{ik}}, \quad (4)$$

where  $T_{ij}$  is the  $S$ - $P$  time for the  $i$ th event at the  $j$ th station. The  $S$ - $P$  time was used to correct for geometrical spreading because some events had poor depth determinations, and

Table 1  
Parameters for the Earthquakes Used in This Study

Date (yr/mo/d)	HHMMSS	$M_L$	Lat	Long	Depth (km)	Event ID
94/01/28	20:09:53.4	4.2	34.38	-118.49	0.7	3146983
94/01/28	20:11:05.1	3.9	34.37	-118.50	0.2	3147036
94/01/29	11:13:18.2	3.4	34.31	-118.41	6.6	3147539
94/01/29	11:20:36.0	5.1	34.31	-118.58	1.1	3147406
94/01/29	11:37:32.3	3.3	34.37	-118.64	12.5	3147246
94/01/29	12:16:56.3	4.3	34.28	-118.61	2.7	3147259
94/01/29	12:21:11.0	3.2	34.29	-118.61	1.8	3147263
94/01/29	12:47:36.2	3.3	34.35	-118.61	13.0	3147272
94/01/29	12:59:43.7	3.1	34.32	-118.56	2.3	3147277
94/01/29	14:03:06.9	3.4	34.30	-118.57	2.3	3147344
94/01/29	21:45:14.0	3.0	34.31	-118.47	7.8	3147443
94/01/30	09:19:56.5	3.3	34.32	-118.55	1.2	3147655
94/01/30	10:44:40.5	3.3	34.38	-118.57	2.5	3147842
94/01/31	04:55:50.3	3.4	34.29	-118.62	2.4	3148020
94/02/01	06:08:20.0	3.0	34.23	-118.59	18.8	3148401
94/02/01	07:40:20.0	3.6	34.23	-118.62	3.7	3148411
94/02/01	08:59:11.0	3.2	34.33	-118.69	4.2	3148450
94/02/02	11:24:37.9	3.8	34.29	-118.61	0.9	3148720
94/02/03	16:23:35.4	4.0	34.30	-118.44	9.0	3149105
94/02/04	04:49:46.0	3.0	34.30	-118.41	6.0	3149297
94/02/04	06:33:39.5	3.5	34.28	-118.62	2.3	3149315
94/02/04	14:26:06.0	3.3	34.27	-118.40	4.1	3149474
94/02/04	20:15:51.9	3.0	34.31	-118.44	6.6	3149534
94/02/05	21:18:41.0	3.0	34.12	-118.49	6.3	3149895
94/02/06	10:00:21.1	3.2	34.38	-118.66	11.3	3150067
94/02/06	13:19:27.0	4.1	34.29	-118.48	9.3	3150210
94/02/06	13:21:45.8	3.6	34.29	-118.48	8.2	3150211
94/02/08	11:16:05.8	3.0	34.34	-118.54	4.9	3150555
94/02/10	07:43:07.1	3.3	34.37	-118.50	2.9	3150980
94/02/10	11:16:12.3	3.5	34.38	-118.49	1.4	3151009
94/02/11	14:07:53.1	3.7	34.33	-118.48	5.0	3151277
94/02/11	15:52:49.2	3.1	34.40	-118.78	10.6	3151303
94/02/14	20:32:57.6	3.2	34.21	-118.56	16.9	3152209
94/02/15	09:42:48.4	3.0	34.37	-118.64	13.8	3152435
94/02/15	12:31:55.3	3.2	34.29	-118.45	6.9	3152592
94/02/16	07:58:42.2	3.2	34.10	-118.51	5.5	3152649
94/02/16	18:00:38.5	3.0	34.29	-118.44	3.0	3152719
94/02/18	09:13:28.4	3.7	34.24	-118.58	16.3	3153233
94/02/18	15:44:23.4	3.1	34.30	-118.45	7.3	3153329

since these events are located very close to some seismic stations, a better distance estimate is obtained from the  $S$ - $P$  time instead of the distance calculated using catalog coordinates.

The horizontal components were treated as a complex signal, as proposed by Tumarkin and Archuleta (1992). According to this method, the sum of the spectral amplitude value corresponding to two symmetric frequencies is calculated. This produces the maximized spectrum (Shoja-Taheri and Bolt, 1977) defined as the maximum amplitude of shaking at a given frequency in the horizontal plane. This eliminates the need to rotate the components and produces results similar to standard averaging methods (Steidl *et al.*, 1995).

The geology of the basin and the source locations directly below the stations make the choice of a reference site

problematic. Station LA00 was selected as a reference site because it is located on mesozoic crystalline rock, and it recorded all the events, making direct spectral ratios possible. The calculated amplifications (or deamplifications) are therefore relative to station LA00.

*Site Amplification from the Inversion of the S-Wave Spectra.* Equation (1) can be rewritten as (e.g., Hartzell, 1992)

$$A_{ij}(f) = S_i(f)R_{ij}^{-\gamma} \exp\left(\frac{-\pi R_{ij}f}{Q_s(f)\beta}\right) G_j(f)I_j(f), \quad (5)$$

where  $S_i(f)$  is the source term of the  $i$ th event,  $R_{ij}$  is the hypocentral distance between the  $j$ th station and the  $i$ th event,  $G_j(f)$  is the site term for the  $j$ th station,  $I_j(f)$  is the instrument response term for the  $j$ th station,  $\gamma$  is the geometrical spreading factor,  $Q_s(f)$  is the average quality factor, and  $\beta$  is the average velocity of the shear waves along the propagation path.

Because the data have been corrected using  $S$ - $P$  times for the geometrical spreading factor, and the instrument response was removed, equation (5) can be rewritten as follows:

$$A_{ij}(f)T_{ij} = S_i(f)k \exp\left(\frac{-\pi T_{ij}f}{Q_s(f)k\beta}\right) G_j(f), \quad (6)$$

where  $T_{ij}$  is the  $S$ - $P$  time for the  $i$ th event at the  $j$ th station;  $\gamma$  has been assumed to be 1;  $k$  is the multiplier factor such that  $T_{ij} = kR_{ij}$ ,  $k = 1/\beta - 1/\alpha$ ; and  $\alpha$  is the average velocity of the longitudinal  $P$  waves along the propagation path.  $\beta$  was assumed to be 3.4 km/sec. The value of  $k$  was obtained from the linear regression of  $T_{ij} = kR_{ij}$  using the hypocentral solutions in Table 1. Based on these results,  $k$  was taken to be 1/6.0.

By taking the natural logarithm, equation (6) can be written for a fixed frequency as

$$a_{ij} = s_i + g_j - \eta_{ij}Q_s^{-1}, \quad (7)$$

where  $a_{ij} = \ln(A_{ij}T_{ij}/k)$ ,  $s_i = \ln(S_i)$ ,  $g_j = \ln(G_j)$ , and  $\eta_{ij} = \pi T_{ij}f/k\beta$ .

Equation (7) can be expressed in matrix form as

$$\mathbf{Dm} = \mathbf{d}, \quad (8)$$

where  $\mathbf{m}$  is a vector in the model space, whose elements consist of  $\eta_{ij}Q_s^{-1}$  and each  $s_i$  and  $g_j$ ;  $\mathbf{d}$  is a vector in the data space, consisting of  $a_{ij}$ ; and  $\mathbf{D}$  is a matrix that relates  $\mathbf{m}$  to  $\mathbf{d}$  through equation (7). The logarithm of the site-amplification factor at LA00 was constrained to 0.0, irrespective of frequency, in order to resolve an indeterminate degree of freedom as well as to compare directly the  $S$ -wave site response with the previous methods. However, to investigate a multi-reference method, the inversion was also recomputed

Table 2  
Instrument Characteristics of the Stations Used in This Study.

Station	Lat	Long	Array	Sensor	Logger	SR	Geol	Tgeol
PDAM	34.2977	-118.3969	NORT	STS-2,FBA23	16,24-bit RT72A-02	200	M	Mxb
NHFS	34.1988	-118.3978	NORT	STS-2	16,24-bit RT72A-02	200	Q	Qyc
SCFS	34.3850	-118.4137	NORT	STS-2	16,24-bit RT72A-02	200	T	
SFPW	34.2990	-118.4380	NORT	CMG3,FBA23	16-bit RT72A-02	100	Q	Qym
LA01	34.1317	-118.4394	NORT	L4C,FBA23	16-bit RT72A-02	200	T	Tss
LA00	34.1062	-118.4542	NORT	L4C,FBA23	16-bit RT72A-02	200	M	Mxb
SFMI	34.2707	-118.4612	NORT	L4C,FBA23	16-bit RT72A-02	250	Q	Qyf
KSRG	34.0596	-118.4737	NORT	STS-2	16-bit RT72A-02	200	Q	Qom
JFPP	34.3120	-118.4960	NORT	L4C,FBA23	16-bit RT72A-02	250	Q	Qym
CSNR	34.2395	-118.5317	NORT	L4C,FBA23	16-bit RT72A-02	250	Q	Qyf
NWHP	34.3882	-118.5347	NORT	L4C,FBA23	16-bit RT72A-02	250	Q	
NMHP	34.2315	-118.5507	NORT	L4C	16-bit RT72A-02	250	Q	Qyf
RESB	34.2968	-118.5507	NORT	L4C,FBA23	16-bit RT72A-02	250	T	Tss
NFCN	34.2412	-118.5547	NORT	L4C,FBA23	16-bit RT72A-02	250	Q	Qym
CWHP	34.2590	-118.5727	NORT	L4C,FBA23	16-bit RT72A-02	250	Q	Qym
CPCP	34.2120	-118.6010	NORT	L22	16-bit RT72A-02	200	Q	Qyf
BRCY	34.3073	-118.6025	NORT	L4C,FBA23	16-bit RT72A-02	250	T	
SMIP	34.2640	-118.6660	NORT	L22	16-bit RT72A-02	200	T	
BCPP	34.2083	-118.6833	NORT	L22	16-bit RT72A-02	200	M	
SSAP	34.2310	-118.7130	NORT	L4C	16-bit RT72A-02	250	T	Tb
PIRU	34.4127	-118.7963	NORT	L4C,FB23	16-bit RT72A-02	250	T	
MPKP	34.2880	-118.8810	NORT	L4C	16-bit RT72A-02	250	Q	
FLMR	34.4118	-118.9322	NORT	CMG5	16-bit RT72A-02	250	Q	
CALB	34.1401	-118.6284	TERR	STS-2,FBA23	24-bit TERRAscope	20,80	T	Tss
PAS	34.1484	-118.1711	TERR	STS-1	24-bit TERRAscope	20	M	Mxb
USC	34.0191	-118.2859	TERR	STS-2,FBA23	16-bit GEOS	20,80	Q	Qym
VRD	34.2145	-118.2796	SCSN	L4C	16-bit SCSN	100	M	Mxb
SMF	34.0123	-118.4465	SCSN	L4C	16-bit SCSN	100	Q	Qym
SYL	34.3536	-118.4509	SCSN	L4C	12-bit SCSN	100	Q	Qym
GRH	34.3088	-118.5588	SCSN	L4C	12-bit SCSN	100	T	
NHL	34.3918	-118.5987	SCSN	L4C	12-bit SCSN	100	Q	

NORT = SCEC portable deployment. TERR = TERRAscope network, and SCSN = Southern California Seismic Network. SR = sampling rate in samples per second. The geology is taken from the digital 1:750,000 map for southern California (M = Mesozoic and older rocks, T = Tertiary age sediments and igneous rocks—chiefly volcanics, Q = Quaternary sediments). Tgeol is the detailed geology from the Quaternary map for the Los Angeles and San Fernando regions (Tinsley and Fumal, 1985).

by constraining the logarithm of the average of the site amplification of six rock sites (LA00, BCPP, SSAP, PDAM, PAS, and VRD) to 0.0.

The inversion is executed solving equation (8) in the least-squares sense subject to the constraint values above. The least-squares solution was determined for each frequency using the singular value decomposition method. The standard deviations of the model parameters were estimated from diagonal elements of the covariance matrix (Menke, 1989)

$$[\text{covm}] = \sigma_d^2 [\mathbf{D}^T \mathbf{D}]^{-1}, \quad (9)$$

where  $\sigma_d^2$  is the variance of the data.

The data for the inversion consisted of the same spectra from the 10-sec window of the *S* wave as used in the direct spectral ratio analysis. The advantage of using inversion methods is that it is possible to include  $Q_s$  as one of the model parameters to be determined, and it is possible to

constrain the reference sites even when those stations have not recorded all the events.

#### Site Amplification from Coda Waves

*Direct Spectral Ratios.* From the single-scattering model of Aki and Chouet (1975), the time- and frequency-dependent amplitude of the coda waves can be expressed as

$$A_{ij}(f, t) = S_i(f) G_j(f) I_j(f) C(f, t), \quad (10)$$

where  $A_{ij}(f, t)$  is the Fourier amplitude of a coda wave for the *i*th event recorded at the *j*th station for a lapse time *t* greater than about twice the *S*-wave travel time of the farthest station used in the analysis.  $S_i(f)$  is the source term of the *i*th event,  $G_j(f)$  is the site term of the *j*th station,  $I_j(f)$  is the instrument response term at the *j*th station, and  $C(f, t)$  is the path term that is independent of source and station. By removing the instrument response first, the relative site amplification between two stations *j* and *k* (in which *k* is the reference station) is given by

Table 3  
Matrix Showing the Events Recorded by Each Station Used in This Study

Event ID	BCPP	BRCY	CALB	CPCP	CSNR	CWHP	FLMR	GRH	JFPP	KSRG
3146983		X	X	X	X	X		X	X	X
3147036		X			X	X		X		
3147539		X	X	X	X	X		X	X	X
3147406		X	X	X	X	X	X		X	
3147259				X	X	X	X	X	X	X
3147263		X		X	X	X			X	
3147272		X	X	X	X	X	X	X	X	X
3147277		X	X	X	X	X		X	X	X
3147344		X	X	X	X	X		X	X	X
3147443			X		X	X		X	X	X
3147655	X	X	X	X	X	X	X	X	X	X
3147842	X	X		X	X	X		X	X	X
3148020	X	X	X	X	X	X	X	X	X	X
3148401	X	X	X	X	X	X	X	X	X	X
3148411	X	X	X	X	X	X	X	X	X	X
3148450	X	X		X		X		X	X	X
3148720	X	X	X	X	X	X	X	X	X	X
3149105		X		X	X	X	X		X	X
3149297	X	X			X	X		X	X	X
3149315	X	X	X	X	X	X	X	X	X	X
3149474	X	X	X	X	X	X		X	X	X
3149534	X	X	X		X			X	X	X
3149895	X	X	X	X	X	X		X	X	X
3150067	X	X	X	X	X	X		X	X	X
3150210	X	X	X	X	X	X		X	X	X
3150211	X	X	X	X	X	X		X	X	X
3150555		X	X	X		X		X	X	X
3150980		X	X	X		X		X	X	X
3151009		X	X	X		X			X	X
3151277							X			X
3151303								X		
3152209		X	X					X		X
3152435		X	X							
3152592			X				X	X		
3152649		X	X							
3152719			X							
3153233		X	X				X	X		
3153329		X	X					X		

(continued)

$$\frac{A_{ij}(f,t)}{A_{ik}(f,t)} = \frac{S_i(f)G_j(f)C(f,t)}{S_i(f)G_k(f)C(f,t)} = \frac{G_j(f)}{G_k(f)}, \quad (11)$$

where  $t$  is the same lapse time for both stations. The assumption in equation (11) is that the coda decay curve  $C(f,t)$  is the same for all source-station pairs. As in the  $S$ -wave direct spectral ratios, station LA00 is the reference site, and the horizontal components were treated as a complex signal. In addition, the direct spectral ratio of the vertical component was also calculated.

**Coda Decay.** Following Aki and Chouet (1975), the coda decay curve is expressed as

$$C(f,t) = t^{-1} \exp(-\pi f t / Q_c), \quad (12)$$

where  $Q_c$  is the quality factor of the coda waves. In order to

apply equation (11), it is necessary to have a common coda decay  $C(f,t)$ , which essentially means that  $Q_c$  is the same for all the stations. The lapse time should be long enough such that the seismic energy can be assumed to be uniformly distributed under the sites of interest. Mayeda *et al.* (1991) and Koyanagi *et al.* (1992) studied different lapse times in order to determine the requirements for the coda decay to be stable for all stations for the same event. They found that the later the lapse time, the better the stability of  $Q_c$ . Unfortunately, the record lengths for the Northridge aftershocks are not very long, so the lapse time was set as three times the travel time of the  $S$ -wave of the farthest station in each event, as suggested by Margheriti *et al.* (1994). The spectral amplitudes for 5-sec windows with 25% overlap were fitted to equation (12) for seven different lapse times in order to compute  $Q_c$ . A pre-event noise window of 5 sec was taken, and only data with signal-to-noise ratio greater than 3 were

Table 3

Matrix Showing the Events Recorded by Each Station Used in This Study (*continued*)

Event ID	LA00	LA01	MPKP	NFCN	NHFS	NHL	NMHP	NWHP	PAS	PDAM
3146983	X	X	X		X	X		X	X	X
3147036	X	X	X			X		X		
3147539	X	X	X		X	X		X	X	X
3147406	X	X	X			X		X	X	X
3147259	X	X	X		X	X		X		
3147263	X	X	X					X		
3147272	X	X	X			X		X	X	X
3147277	X		X		X			X		X
3147344	X	X	X					X	X	X
3147443	X	X	X		X	X		X		X
3147655	X		X		X	X		X	X	X
3147842	X	X	X		X	X		X	X	X
3148020	X	X	X			X		X		
3148401	X	X	X			X		X	X	
3148411	X	X			X	X		X	X	X
3148450	X	X	X		X	X		X	X	
3148720	X	X	X		X	X		X	X	X
3149105	X	X	X					X		
3149297	X	X	X					X		
3149315	X	X	X		X	X		X	X	X
3149474	X	X			X			X	X	X
3149534	X	X							X	
3149895	X	X			X	X			X	
3150067	X	X	X		X	X		X	X	
3150210	X	X	X		X	X		X	X	X
3150211	X	X	X		X	X		X	X	X
3150555	X		X		X	X		X		X
3150980	X	X	X	X		X	X	X	X	
3151009	X	X	X	X	X		X	X	X	X
3151277	X	X	X	X		X		X	X	
3151303	X	X				X	X			
3152209	X	X	X	X		X	X	X	X	
3152435	X		X	X			X			
3152592	X	X		X			X	X	X	
3152649	X	X	X	X			X		X	
3152719	X	X		X			X		X	
3153233	X	X		X		X	X	X		
3153329	X	X	X	X			X			

*(continued)*

used. Figure 3 shows the averaged  $Q_c^{-1}$  for all stations and components. It is observed that there is a common coda decay in the San Fernando basin at this lapse time. In addition, the three components have almost the same decay; however, it is also observed that there is scattering in the values of  $Q_c^{-1}$ . This variation of  $Q_c^{-1}$  among stations might be explained by the complex configuration of the San Fernando basin, with the presence of the Santa Monica mountains to the south, which separate the San Fernando basin from the Los Angeles basin, and the Santa Susana mountains to the north. This geological setting produces reverberations and trapped waves in the San Fernando basin (Olsen and Archuleta, 1996). In addition, the hypocentral distances are short, and many events are shallow, so surface-wave energy might still be within the coda window. In spite of the variability of  $Q_c^{-1}$ , the spectral ratios are computed, and the results will be examined in the next sections.

*Inversion of the Coda-Wave Spectra.* Equation (10) shows that the coda waves can be represented as the convolution of the source, the instrument, the coda decay, and the site term. Since the instrument response was removed, and by taking natural logarithms, equation (10) can be rewritten as

$$a_{ij} = cs_i + g_j, \quad (13)$$

where  $a_{ij} = \ln(A_{ij})$ ,  $cs_i = \ln(CS_i)$ , and  $g_j = \ln(G_j)$ . The source and the coda decay terms remain convolved since this study is interested in the site term only.

Equation (13) is solved by using the same procedure as for the inversion of the *S*-wave spectra. However, to check the stability of the horizontal and the vertical coda site amplification in terms of the chosen reference site, the constraints to solve (13) were set up with each rock site equal to 0.0 first. Finally, the logarithm of the average of the six

Table 3  
Matrix Showing the Events Recorded by Each Station Used in This Study (*continued*)

Event ID	PIRU	RESB	SCFS	SFMI	SFPW	SMF	SMIP	SSAP	SYL	UCS	VRD
3146983	X	X		X	X	X		X	X	X	X
3147036		X		X	X	X		X	X		X
3147539	X	X		X	X	X	X	X	X	X	X
3147406	X	X		X	X	X	X	X	X	X	X
3147259	X	X		X	X	X	X	X		X	
3147263		X		X			X				
3147272	X	X		X	X	X	X	X	X	X	X
3147277	X	X		X	X		X	X	X		X
3147344	X	X		X	X		X	X	X		X
3147443	X			X	X	X	X	X	X		X
3147655	X	X		X	X	X	X	X	X		X
3147842	X	X		X	X	X	X	X	X		X
3148020	X	X		X	X	X	X	X	X		X
3148401	X	X		X	X	X	X	X	X		X
3148411	X	X		X	X	X	X	X	X	X	X
3148450	X	X		X	X	X	X	X	X		
3148720	X	X		X	X		X	X	X	X	X
3149105		X		X	X		X				
3149297	X	X		X	X		X	X	X		X
3149315	X	X	X	X			X	X	X	X	X
3149474	X	X	X			X	X	X	X		
3149534	X	X	X	X			X	X	X		
3149895	X										
3150067	X	X	X	X		X	X	X	X		
3150210	X	X	X	X		X	X	X	X	X	X
3150211	X	X	X	X		X	X	X	X		X
3150555	X	X	X	X			X	X	X		
3150980	X				X	X		X	X	X	X
3151009	X		X		X			X		X	
3151277	X				X	X		X		X	X
3151303	X							X			
3152209	X				X			X	X		X
3152435	X		X					X			
3152592	X		X		X	X		X	X		X
3152649	X					X		X	X	X	X
3152719					X			X	X		
3153233					X	X		X	X	X	X
3153329	X				X			X	X		X

rock site responses (LA00, BCPP, SSAP, PDAM, PAS, and VRD) was constrained to 0.0 in order to compare the coda method, using the vertical and horizontal components, with the *S*-wave method.

#### Site Amplification from Receiver-Function Estimates

Receiver-function estimates were introduced by Langston (1979) as a method to study the upper mantle and the crust from teleseismic records. The basic assumption in this technique is that the vertical component is not influenced by the local structure, whereas the horizontal components contain the *P*-to-*S* conversions due to the geology underlying the station. Then by deconvolving the vertical component from the horizontal, the site response is obtained.

In the frequency domain, this formulation is expressed as

$$\frac{H}{V} = \frac{A_{Hij}(f)}{2\sqrt{2}A_{Vij}(f)}, \quad (14)$$

where  $A_{Hij}(f)$  is the maximized spectrum of the *S*-wave window on the horizontal components and  $A_{Vij}(f)$  is the Fourier amplitude of the *S*-wave window on the vertical component for the *i*th event recorded at the *j*th station. The factor of 2 in the denominator reflects the symmetry of the Fourier spectrum of a single component. The maximum amplitude of shaking at a given frequency is twice the amplitude spectrum of a real signal. The factor  $\sqrt{2}$  represents the partition of energy between the horizontal components (e.g., Lachet *et al.*, 1996).



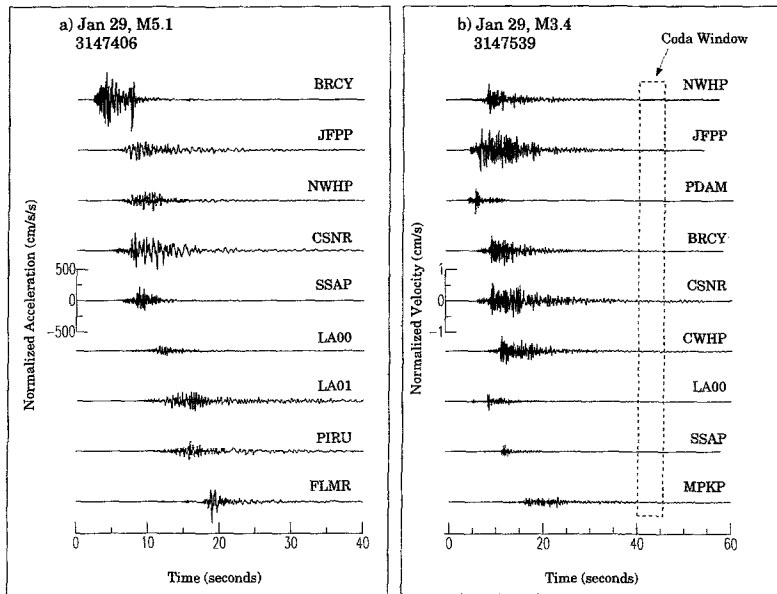


Figure 2. Example of (a) acceleration and (b) velocity time histories for events 3147406 and 3147539, respectively. The acceleration and velocity have been scaled by the  $S$ - $P$  time of each station. The coda window is defined as three times the travel time of the  $S$  wave at the farthest station.

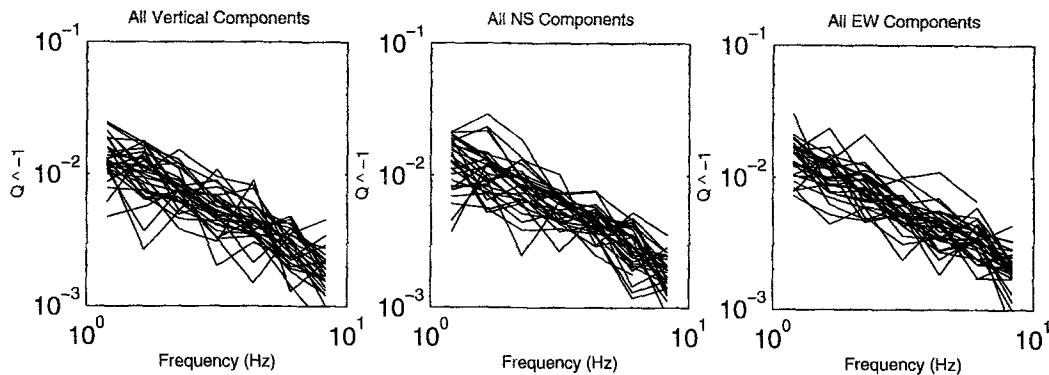


Figure 3. Coda  $Q_c^{-1}$  versus frequency. The lapse time is three times the travel time of the  $S$  wave at the farthest station. The value of  $Q_c^{-1}$  is an average over all the events for each station. Note that the three components have almost the same  $Q_c(f)$  decay, but the coda  $Q_c^{-1}$  values are still not completely stable for the chosen lapse time.

## Results

Three time windows were considered for the calculation of the Fourier spectra of the records. The portions of the seismograms used consisted of a 5-sec window of the coda, a 10-sec window for the  $S$  wave starting 2 sec before its arrival, and a 40-sec window containing almost the whole record, starting 1 sec before the  $P$ -wave arrival. The first window was extracted from velocity records, and the last two windows were extracted from both velocity and acceleration records, depending on the strength of the signal. A 5% Hanning taper was applied to all time windows. A pre-event noise window of 5 sec was also taken. The spectra of the noise and the actual data were smoothed and reinterpolated to a common frequency interval, and only data with signal-to-noise ratio greater than 3 were used to compute the spectral ratios. The smoothing was done using a rectangle function 0.5 Hz wide. Once the direct spectral ratio for each

station and each earthquake was obtained, the logarithmic average and the 95% confidence limits of the mean were calculated.

Figures 4 to 7 show the site amplification as a function of the frequency for each station. The solid line is the average, and the dotted lines are the 95% confidence limits. Station GRH was used only to calculate coda amplifications because its records usually were clipped during the  $S$ -wave window.

Figure 4 shows the site-amplification factor obtained from the inversion of the  $S$ -wave spectra using the average of six rock sites (LA00, BCPP, PAS, PDAM, VRD, and SSAP) as a reference. Figures 5 and 6 show the site-amplification factor obtained from the inversion of the coda spectra of the horizontal and vertical components, respectively, using the same averaged reference site as the  $S$ -wave method. Figure 7 shows the amplification factor from the  $H/V$  ratio for each station.

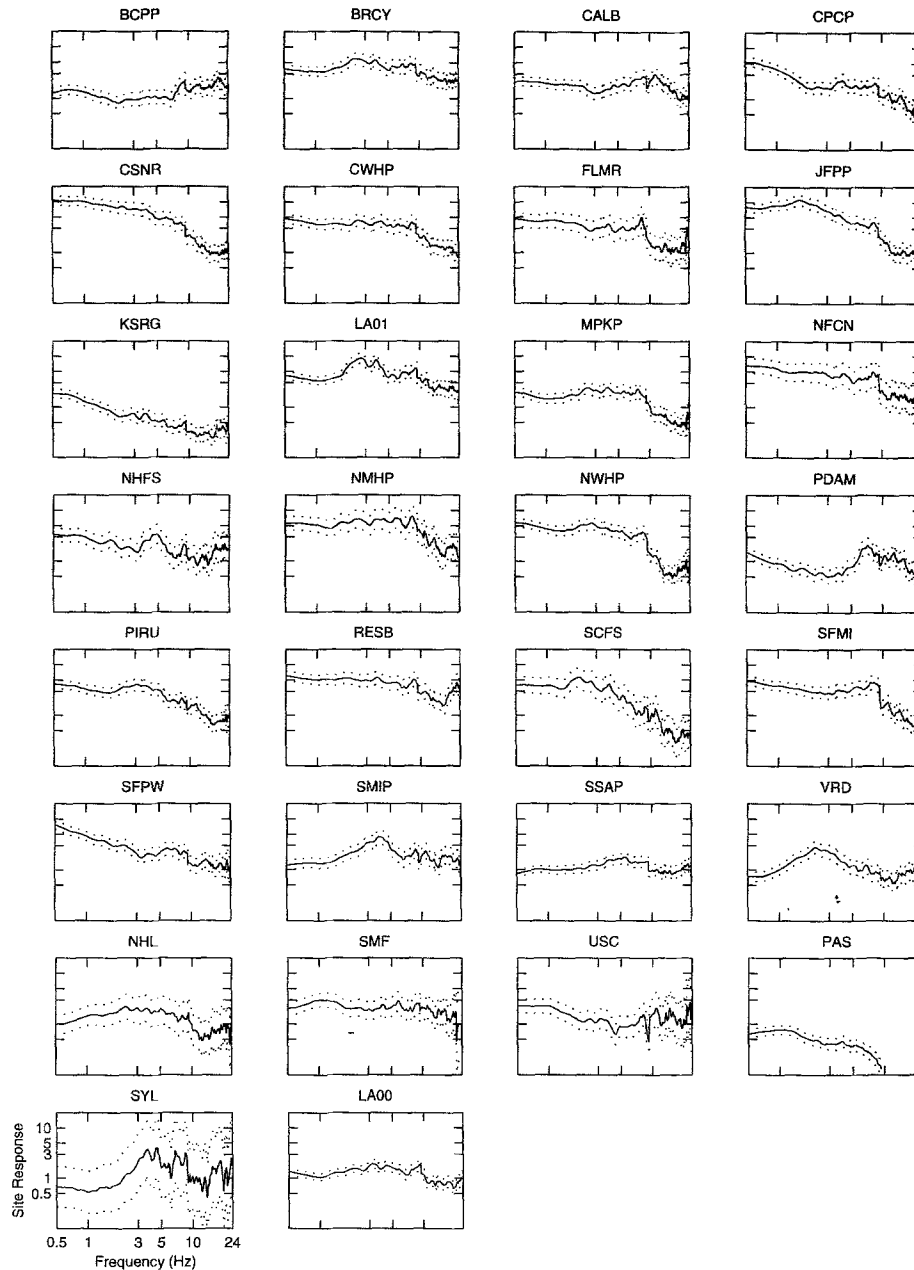


Figure 4. Site response obtained from the inversion of the 10-sec window of the *S*-wave spectra using the average of six rock sites (LA00, PAS, PDAM, BCPP, VRD, and SSAP) as a reference site. Solid lines represent the average, and dotted lines are the 95% confidence intervals.

As shown by the amplification values from Figure 4, in general, stations located within the Northridge and Los Angeles basins (CPCP, CSNR, CWHF, FLMR, GRH, JFPP, MPKP, NFCN, NHFS, NHL, NMHP, NWHP, PIRU, SCFS, SFMI, SFPW, SMF, SMIP, and USC) have the largest amplifications, with values greater than 4 between 0.5 and 3.0 Hz. The frequency corresponding to the maximum amplification value does, however, vary between methods. It is closer to 1.0 Hz for the *S*-wave method and 1.5 Hz for the coda method (Figs. 5 and 6). The stations with the largest amplifications (values of 8 to 10 between 0.5 and 3.0 Hz) are all located on Qua-

ternary young soils corresponding to class Q<sub>y</sub> (see Table 2). These stations are CSNR, JFPP, NFCN, NMHP, and NWHP. Stations located on stiff soil (BRCY, KSRG, LA01, CALB, and RESB, which correspond to class Q<sub>o</sub> + T<sub>s</sub>—Quaternary old and Tertiary sediments—in Table 2) show relatively low amplification values that are two or three times lower than those from the stations in the basins. Finally, the amplification values at the rock sites (LA00, BCPP, PAS, PDAM, VRD, and SSAP, which correspond to class T<sub>b</sub> + M<sub>x</sub>—Tertiary basement and Mesozoic crystalline rock—in Table 2) are generally smaller than the amplification values from

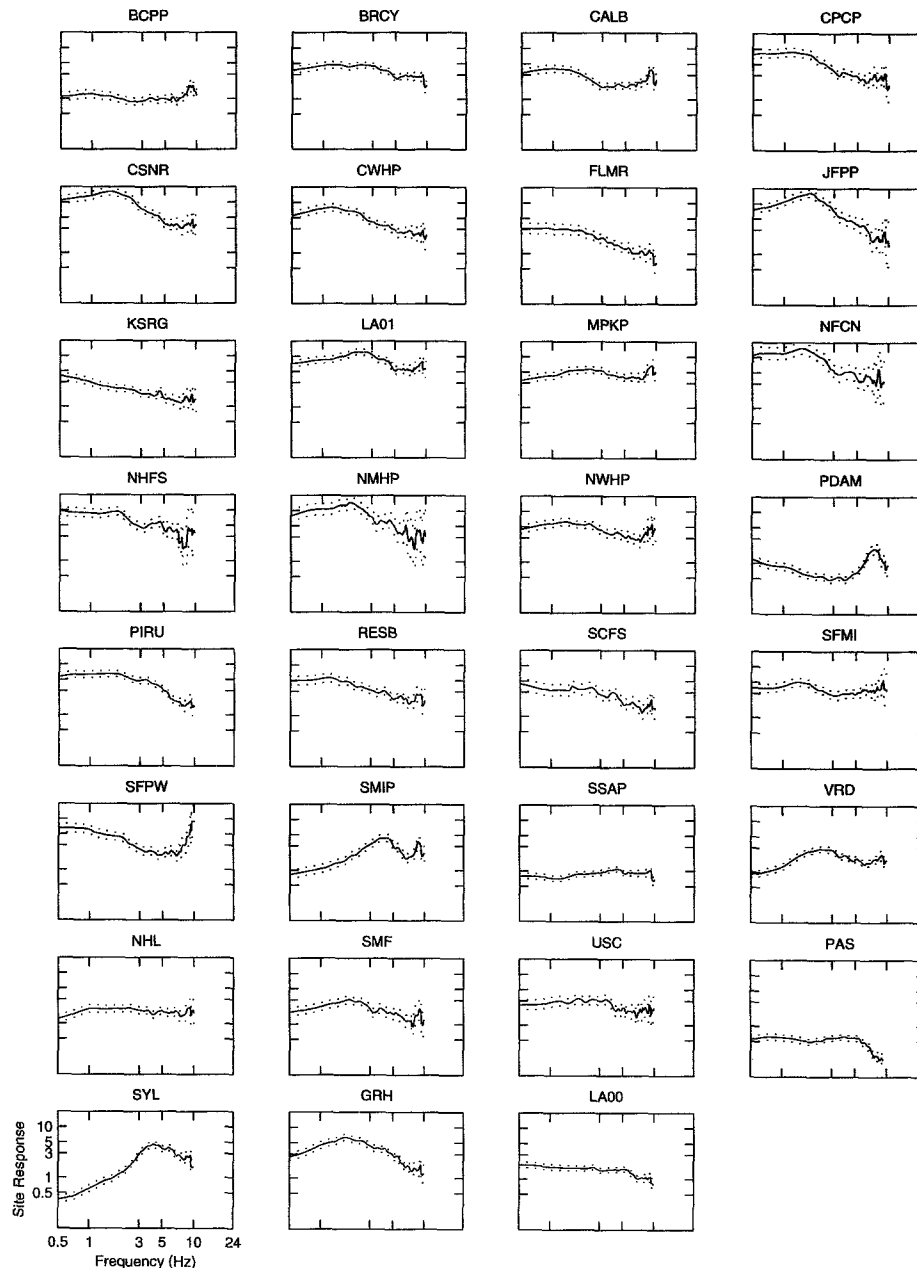


Figure 5. Site response obtained from the inversion of the 5-sec window of the coda window spectra of the horizontal components using the average of the six rock sites as a reference site. The lapse time is the same as it was used to compute the coda  $Q_c$  decay and corresponds to three times the travel time of the  $S$  wave at the farthest station.

the other sites and, as a result of the chosen constraint, are close to 1.0.

The same tendency of larger amplifications in young soil sites and low amplifications in old rock sites is observed using the coda method in Figures 5 and 6. Conversely, the  $H/V$  method (Fig. 7) shows the same predominant peaks at the same frequency as the  $S$ -wave method (thick line); however, the amplification factors are not the same.

In the inversion method (Fig. 4), it is possible to see the

relative site response for each rock site under the constraint that the logarithm of their average is 0.0. For example, PAS shows some deamplification, while VRD shows some amplification. This clearly shows the advantage of using several rock stations rather than one, which may under- or overestimate the relative site response. Nevertheless, it is necessary to recall that these responses are not absolute values but relative responses with respect to the average of the rock sites.

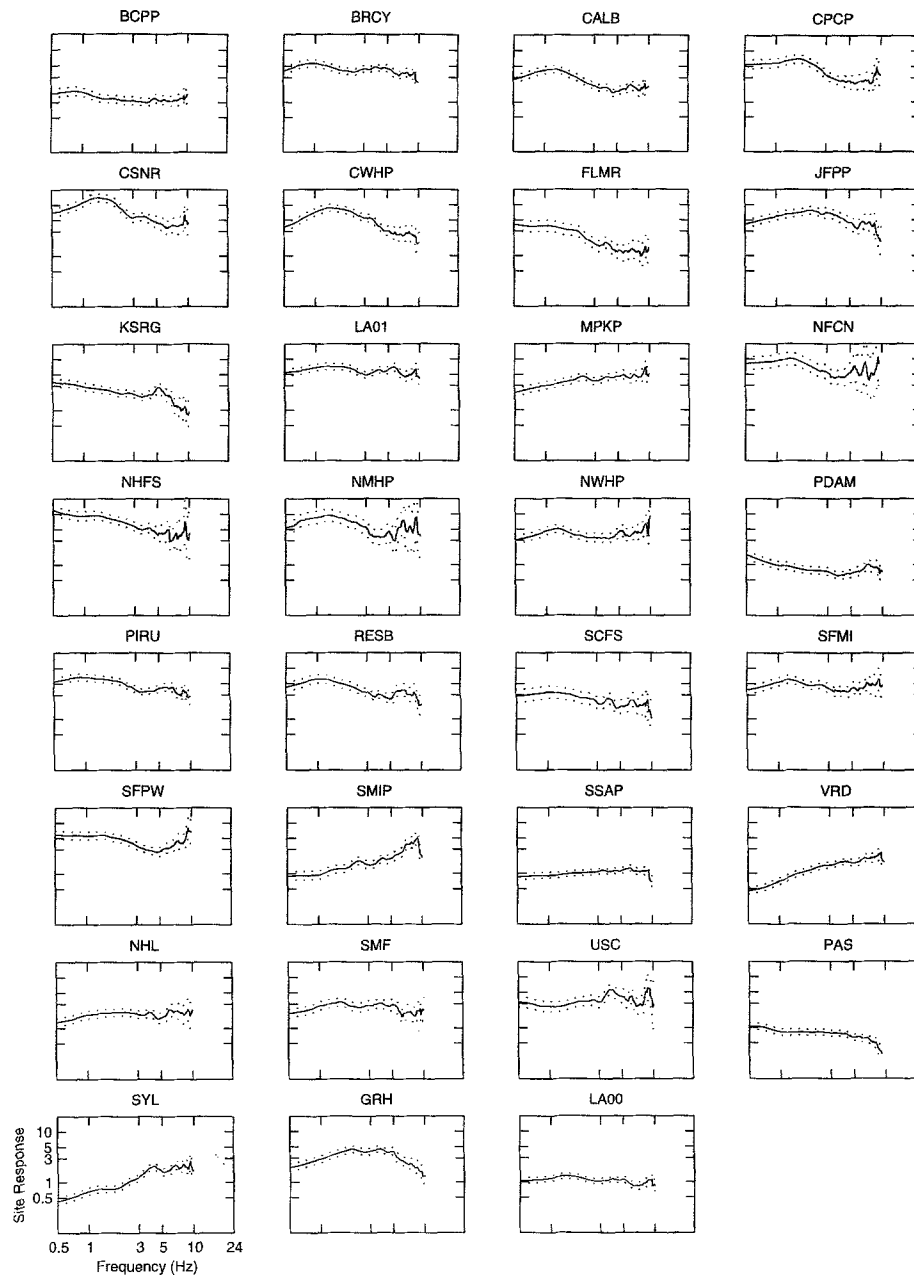


Figure 6. Site response obtained from the inversion of the 5-sec window of the coda window spectra of the vertical components using the average of the six rock sites as a reference site. The lapse time is the same as for the horizontal components.

## Discussion

### Effect of the Time Window Length

Since shear waves typically show large amplification in sediments, and usually cause the most damage in man-made structures, many previous studies have used *S* waves for estimating the site-amplification factor. However, the signal must be long enough so that any resonant peaks in the spectral ratios can be adequately resolved. Therefore, it is necessary to use as much of the signal as possible in order to achieve better spectral resolution. Nonetheless, the longer

the signal segment involved, the more scattering and reflections are included in the signal. This complicates a single model of site amplification for a fixed incidence angle, wave type, and azimuth. However, for seismic hazard evaluation purposes, this might be an advantage because the spectral ratio would represent a smoothed and conservative average of the site amplification over those parameters (Field *et al.*, 1992). Nevertheless, using the whole record makes it difficult to correct for the intrinsic attenuation because of the combination of different wave types. With no whole path *Q* correction, the direct spectral ratios for the different time window lengths are similar. This result indicates that there

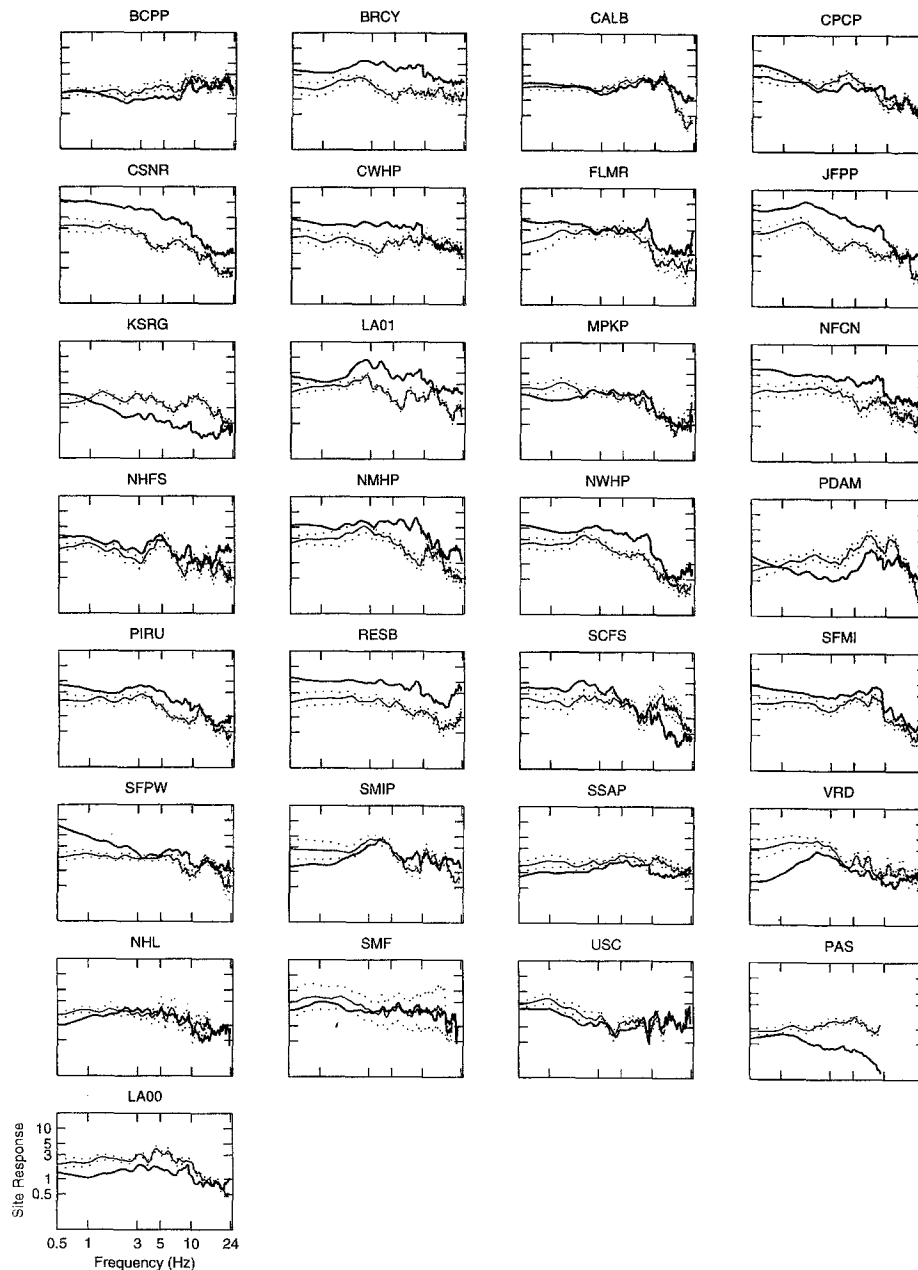


Figure 7. Site response obtained from the  $H/V$  ratios. For comparison, the results from the inversion of the  $S$ -wave spectra using the average of the six stations as a reference site (Fig. 4) have also been plotted. The thin line represents the  $H/V$  ratios, and the thick line represents the inversion. The frequency of the predominant peaks agree with those from the inversion method; however, the amplification values can be quite different. Station SYL was not used because it had only one acceleration recording.

is no statistical difference between 10- and 40-sec time windows for calculating the site amplification.

#### Direct Spectral Ratios Versus Inversion Method on the $S$ Wave

Equation (5) shows that the path term includes both geometrical and the whole path  $Q_s$  attenuation. Since the stations are very close to the events, geometric attenuation, es-

pecially the difference in the hypocentral distance between the reference site and the other sites, is more important than the  $Q_s$  effect. However, for stations far from the earthquakes, the  $Q_s$  attenuation might play an important role, especially at high frequencies. As an example, Figure 8 shows the amplification at stations JFPP and FLMR using the direct spectral ratio and the inversion method with LA00 as the reference site in both methods. The shaded zone represents the

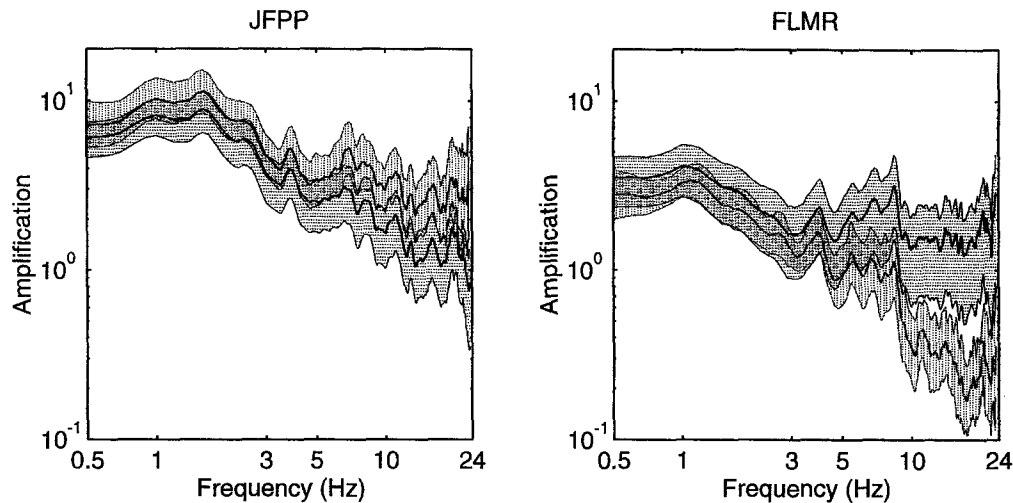


Figure 8. Example of the effect of  $Q_s$  on the calculation of site response. For both the direct spectral ratios and the inversion method, LA00 is the reference site. The shaded zone represents the 95% confidence limits of the mean. Station JFPP, located closer to the events, shows a higher value of the direct spectral ratio (shaded with vertical lines), whereas station FLMR, the farthest station from the events, shows a higher value of the site amplification from the inversion method (shaded with horizontal lines). Although these methods produce statistically the same result for low frequencies (overlapped regions), the difference becomes important at higher frequencies.

95% confidence limits. Station JFPP, located closer to the events, shows a higher value of site amplification when using the direct spectral ratio (shaded with vertical lines), whereas station FLMR, the farthest station from the events, shows a higher value of site amplification when using the inversion method (shaded with horizontal lines). Although these methods produce statistically the same result for low frequencies, the difference becomes important at higher frequencies. This result implies that for analyses of site response where stations are widely distributed, not only geometrical but also whole path attenuation should be considered in calculating the amplification factors.

The inversion method solves for the source,  $Q_s$ , and the site term assuming that the response of the reference station or stations is 1.0, independent of frequency. This assumption implies that the chosen station or stations are good reference sites. However, the computed source spectra are implicitly convolved with the site response of the chosen reference station. Thus, if the reference sites have flat amplitude response, this method separates path and site from source. However, if the reference sites have their own frequency-dependent response (e.g., Steidl *et al.*, 1996), then this response is incorporated into the “source” spectrum when the reference sites are constrained to 1.0. Figure 9 shows the source acceleration spectra computed from the inversion when LA00, BCPP, VRD, SSAP, and PDAM are used as reference sites. The sources follow an  $\omega^2$  model; however, for high frequencies (greater than 10 Hz), the source spectra are not flat, suggesting that the reference sites may have their

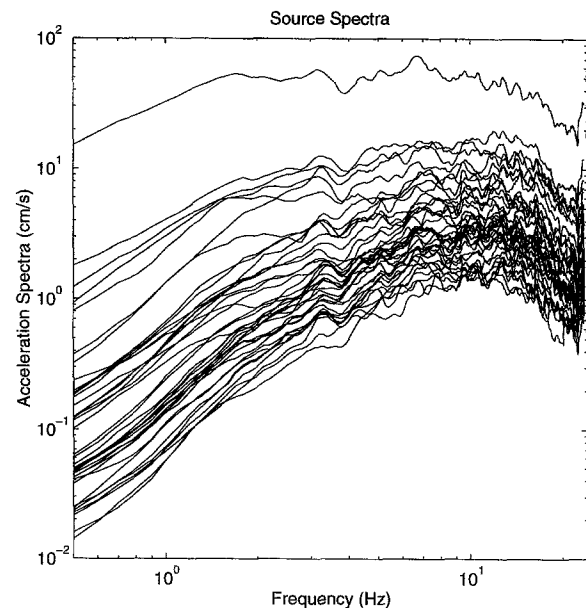


Figure 9. Acceleration source spectra from the inversion of the  $S$ -wave spectra when the average of LA00, PDAM, VRD, SSAP, and BCPP is used as a reference site. The source spectra follow an  $\omega^2$  model; however, their shape is no longer flat for frequencies greater than 10 to 12 Hz. This suggests that the reference sites may have their own site response at those frequencies.

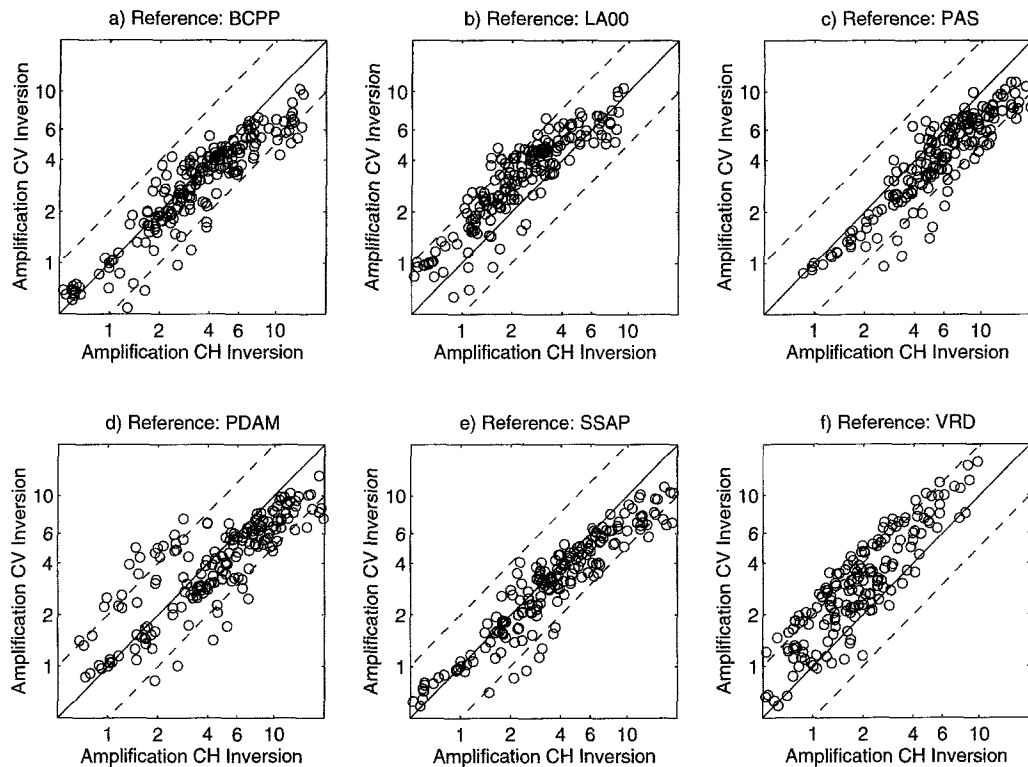


Figure 10. Average amplification at all sites from vertical-component coda window (vertical axis) versus average amplification at all sites from horizontal components coda window (horizontal axis), for all center frequencies (0.75, 1.0, 1.5, 2.0, 3.0, 4.0, and 6.0 Hz). The solid line represents the 1:1 correspondence between the two methods, and the dashed lines represent a factor of 2 of difference between methods. These results are from separate inversions where (a) BCPP, (b) LA00, (c) PAS, (d) PDAM, (e) SSAP, and (f) VRD are constrained to have unity site response. Using a different reference site in each inversion, it is observed how the choice of reference site affects the results.

own response at those frequencies. The decrease in high frequency of the source spectra is interpreted at least in part to amplification of the high frequencies at the reference sites, which have been constrained to 1.0. This amplification has been mapped into the source spectra. This result is consistent with Steidl *et al.* (1996), who have shown that outcrop rock can have its own site amplification by comparing direct spectral ratios using borehole and surface rock data. If there is high-frequency amplification at the reference sites, the high-frequency amplification at soil sites may be underestimated.

Inversions of the *S*-wave spectra of the vertical, radial, and transverse components were also calculated in order to detect any discrepancies with the results obtained from the inversion of the complex representation of the horizontal components. The site response from the vertical components agrees within a factor of 2 with the response from the horizontals; however, the former, in general, produce lower amplification factors than the latter. Conversely, the site response from radial and transverse components agrees with the response obtained from the complex representation of the horizontals. In addition, there is no statistical difference between amplifications from the radial and transverse components, respectively.

#### Inversion of the Coda Spectra Versus Inversion of the *S*-Wave Spectra

In order to compare the methods for estimation of site-amplification factors, the spectral ratio for each method at each station was averaged over seven center frequencies. A bandwidth of  $\pm 0.25$  Hz was used for the center frequency at 0.75 and 1.0 Hz,  $\pm 0.5$  for the center frequency at 1.5 and 2.0 Hz, and  $\pm 1.0$  for the remaining center frequencies at 3.0, 4.0, and 6.0 Hz. Then the averaged amplifications at each center frequency were plotted for the different methods. Figures 10 to 14 summarize the results. The solid line shows a 1:1 correspondence between methods, and the dashed lines show a factor of 2 of difference between methods. The vertical and horizontal bars represent the 95% confidence limits for both methods at the same center frequency.

In order to check whether amplification from the vertical and horizontal components using the coda window depends on the chosen reference site, the coda amplification from the inversion of the coda spectra of the horizontal and vertical components was determined taking a different rock site as a reference site each time. Figure 10 shows the comparison of the horizontal and vertical component average

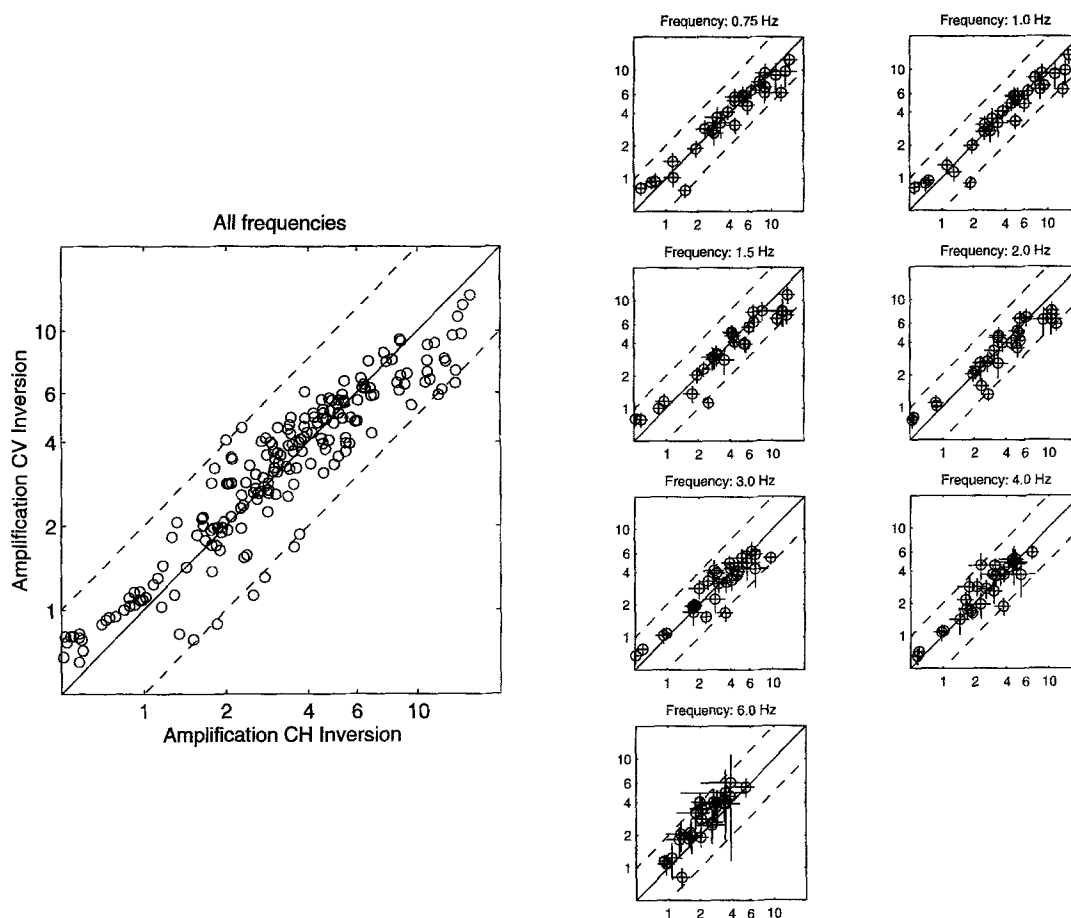


Figure 11. Average amplification at all sites from horizontal-component coda window (CV) versus average amplification at all sites from vertical-component coda window (CH). Average amplification values for all center frequencies (0.75, 1.0, 1.5, 2.0, 3.0, 4.0, and 6.0 Hz) are shown in the large figure. The average of the six rock sites is used as a reference site. The solid line represents the 1:1 correspondence between the two methods, and the dashed lines represent a factor of 2 of difference between methods. The average amplification values for each center frequency are shown individually in the smaller figures along with the 95% confidence limits for both methods at that frequency. The large figure is thus a summation of all the smaller figures. Both methods produce similar results within a factor of 2.

coda amplification factors for all seven center frequencies. Steidl *et al.* (1995) reported that vertical coda site-response estimates were consistently larger than horizontal coda estimates when using LA00 as a reference site. A similar result is found when station VRD is used as a reference site (Fig. 10). However, the opposite result is obtained when BCPP, PAS, PDAM, and SSAP are used as reference sites. Because of this result and to compare with the *S*-wave method, the average of the six stations as a reference site is used to calculate the coda amplification using the coda inversion method.

Figure 11 shows the comparison between average site amplification obtained from the coda window on the vertical component and the coda window on the horizontals using the average of the six stations as a reference site. The amplification values obtained from the vertical component are

similar to those obtained from the horizontals within a factor of 2. This behavior is observed for all frequency ranges. This result indicates that the amplification from the vertical and the horizontal components is similar when a large enough number of stations located on rock is used as an averaged reference site.

Figure 12 compares the average amplification factors obtained from the inverted horizontal coda window and the inverted horizontal *S*-window spectra. The asterisks represent the amplification at the rock sites. The coda method and the *S*-wave method produce results within a factor of 2 to 4 of each other. Figure 13 shows the average amplification factors from the inverted vertical coda window and the inverted *S*-window spectra. The vertical coda method estimates are also close to the estimates from the *S*-wave method within a factor of 2 to 4. However, Figures 12 and 13 show



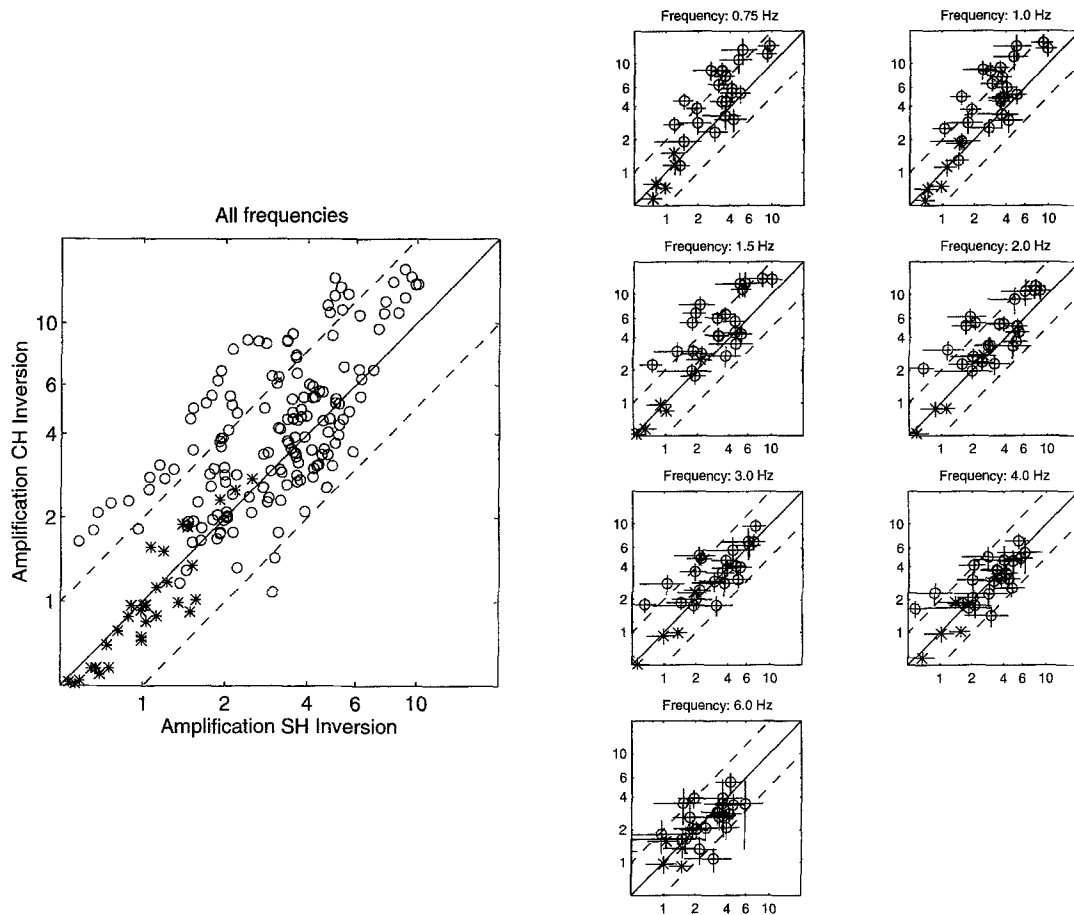


Figure 12. Average amplification at all sites from horizontal-component coda window (CH) versus average amplification at all sites from horizontal  $S$  window (SH) using the average of the six rock sites as a reference site. Asterisks represent the amplification at the rock sites. Amplifications from the horizontal coda window are in some cases more than twice those obtained from the horizontal  $S$  window, especially at frequencies of 2 Hz and lower for nonrock sites (open circles).

that the coda method and the  $S$ -wave method do not always produce the same result, especially for stations located on nonrock sites (open circles), where the coda method shows larger amplifications than the  $S$  wave in many cases. This behavior was also shown in Margheriti *et al.* (1994), Steidl *et al.* (1995), and Field (1996). These studies found amplifications generally higher for the coda-wave estimates. One possible explanation for this is basin-trapped waves present late in the records. As shown previously, the  $Q_c^{-1}$  has some variability that could be explained by the basin-trapped waves and suggests that the assumption regarding common coda decay may not always hold for basin or near-basin sites. Phillips and Aki (1986) and Frankel (1993) have suggested that coda amplification might be larger because of the seismic energy trapped in alluvial basins. Thus, stations close to the basin or in the basin may have relatively larger amplifications with respect to reference sites because the latter do not have trapped basin energy in their signal. Finally, because most of the data represent relatively weak motion, the issue of nonlinear site response is not addressed here. How-

ever, studies that predict strong ground motion based on vertical coda-wave amplification factors may be overestimating the predicted ground motion.

#### $H/V$ Ratios Versus Inversion of the $S$ -Wave Spectra

The  $H/V$  ratio method as a measure of the site response was introduced by Lermo and Chávez-García (1993), where they compared the  $S$ -wave and  $H/V$  ratios for several sediment sites in Mexico. They found that the  $H/V$  method is able to identify the resonant frequency and its associated amplification value comparably to the  $S$ -wave method. However, Field and Jacob (1995) showed that while the fundamental frequency can be resolved, the amplification had a discrepancy of about 1.6 compared to the  $S$ -wave method. Recent studies (Lachet and Bard, 1994; Lachet *et al.*, 1996; Field, 1996) have shown that, in general, the resonance frequency obtained from  $H/V$  ratios is statistically similar to the one from the  $S$ -wave technique; nevertheless, the amplification is very different from that of the  $S$ -wave method.

Figure 14 shows the average amplification factors from

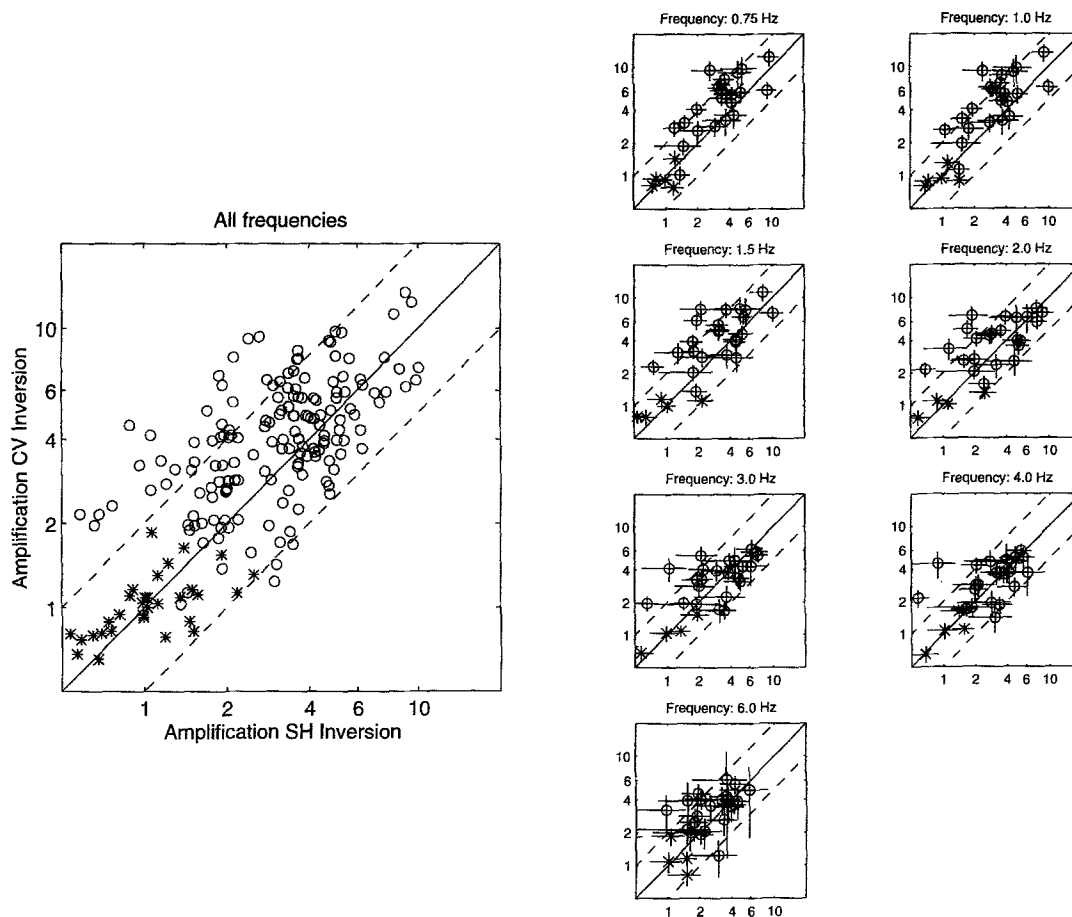


Figure 13. Average amplification at all sites from vertical-component coda window (CV) versus average amplification at all sites from horizontal *S* window (SH) using the average of the six rock sites as a reference site. Asterisks represent the amplification at the rock sites. Amplifications from the vertical coda window of nonrock sites (open circles) are in some cases more than twice those obtained from the horizontal *S* window for all frequencies.

the inversion of the *S*-wave spectra using the six rock stations as a reference site and from the *H/V* ratio. The amplifications determined from the *H/V* method show a weak correlation with the amplifications determined from the *S*-wave inversion. In addition, from Figure 7, the *H/V* ratios seem to be useful for extracting peak frequencies of the site response, but not for estimating the amplification factors. Finally, since the vertical and horizontal components have similar site amplification, the fundamental assumption of the *H/V* method (vertical component free of site response) is broken, and, consequently, this technique fails to reproduce the site amplification of the *S* waves.

#### Relation with the Geology

In order to investigate the variation of the site response with surface geology, the sites were divided into three classes from two different sources: (1) The general classification based on the 1:750,000 geology map of California and (2) the detailed classification based on the Quaternary geologic map for the Los Angeles region (Tinsley and Fu-

mal, 1985). The general classes are Quaternary, Q, Tertiary, T, and Mesozoic, M. The detailed classes are separated as follows: The first class combines all Mesozoic and Tertiary basement units and is denoted as Tb + Mx. The second class, Qo + Ts, is comprised of Pleistocene alluvium and Tertiary sediments. Finally, Holocene units all belong to the Qy class (see Table 2). This separation was based on the average shear-wave velocity in the upper 30 m for the different classes (Park *et al.*, 1996).

Figures 15a and 15b show the logarithmic average amplification obtained for the general and detailed geology classifications, respectively. Stations without classification in both general and detailed geology were not used to compute the average. The thick line represents the site response for Tb + Mx and Mesozoic classes. The thin line represents the Qo + Ts and Tertiary classes. The dashed line represents the Qy and Quaternary classes. In addition, Table 4 lists the mean amplification and the standard deviation of the mean for 1.0, 3.0, and 10.0 Hz. Since station PAS had no data above 8.0 Hz, and in order to calculate the average site re-

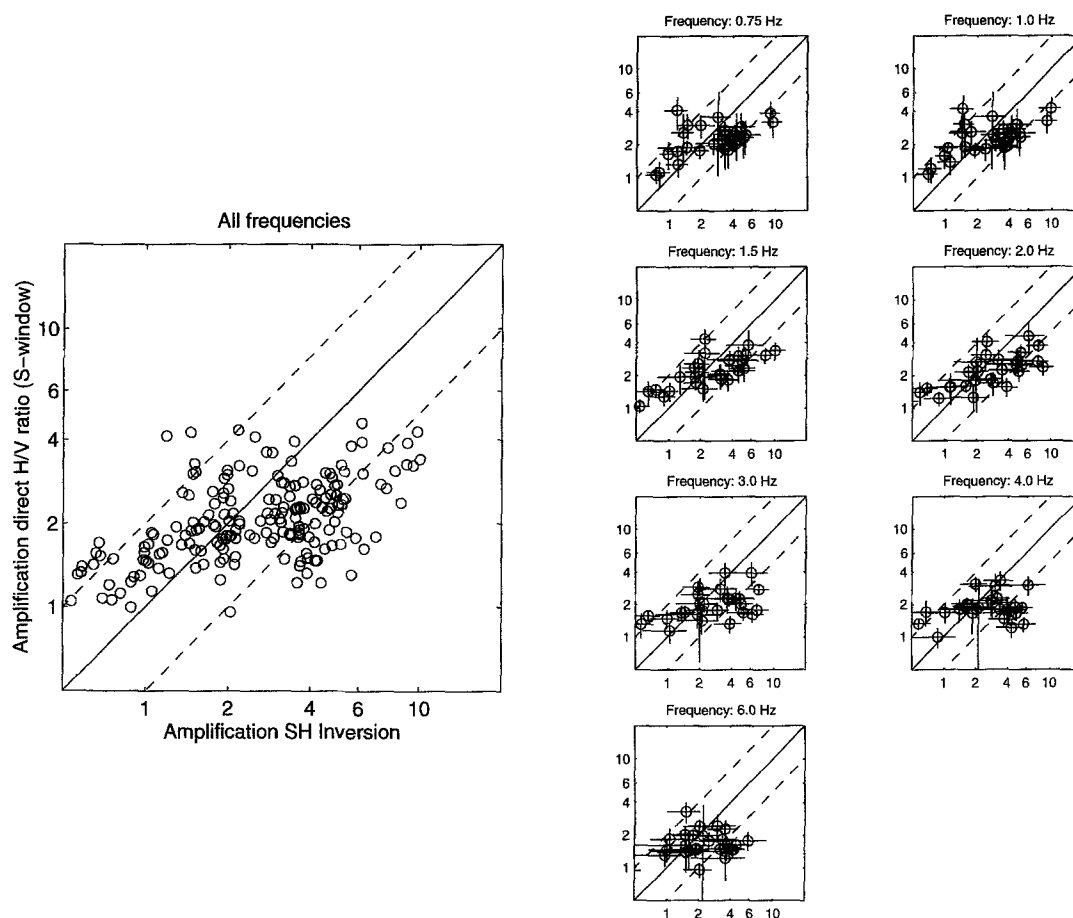


Figure 14. Average amplification at all sites from  $H/V$  ratios (vertical axis) versus average amplification at all sites from horizontal  $S$  window (horizontal axis) using the average of the six rock sites as a reference site. Amplifications from  $H/V$  ratios are consistently different from those obtained from the horizontal  $S$  window, and there is little correlation between methods.

sponse up to 24 Hz for each class using a consistent constraint at all frequencies, the inversion of the  $S$ -wave spectra was performed using the average of the remaining five rock stations as a reference site. These five stations make up the Tb + Mx class, and for this reason, the Tb + Mx class has an average value of 1.0 (Fig. 15b) as required by the inversion constraint. Station PAS was excluded in calculating the Tb + Mx and M means.

Since the reference sites show their own site response and the measured site amplification is underestimated at high frequencies, the difference in site response between the different classifications is small at high frequencies, as shown in Figure 15. However, the detailed geology classification distinguishes more clearly at the lower frequencies the average site response for each class than the general geology classification. The general geology classification does not distinguish the site response on the Quaternary from the Tertiary except for frequencies below 2.0 Hz. The only difference between Figures 15a and 15b is from stations SSAP and KSRG. Station SSAP goes from T to Tb + Mx, and station KSRG goes from Q to Qo + Ts. This overlapping between the Tertiary and Quaternary is mainly because of the pres-

ence of station KSRG in the Quaternary class, having a lower site response relative to the other Quaternary stations (Fig. 4), which lowers the average Quaternary amplification in Figure 15a. At the same time, the site response at station SSAP shows some high-frequency amplification (Fig. 4), which raises the average Tertiary amplification in Figure 15a. The combination of these two stations produces the difference between Figures 15a and 15b. Due to the small number of observations for each class, the standard deviation of the mean is quite high (see Table 4); therefore, it cannot be said statistically that one classification is better than the other. While it is encouraging that the mean amplification between the detailed classes separates, the large uncertainties show that it is necessary to collect more data at sites with detailed surface geology information in order to characterize better the average site amplification of each class.

## Conclusions

The coda,  $S$ -wave, and  $H/V$  site amplifications in the San Fernando Valley were evaluated using 38 aftershocks

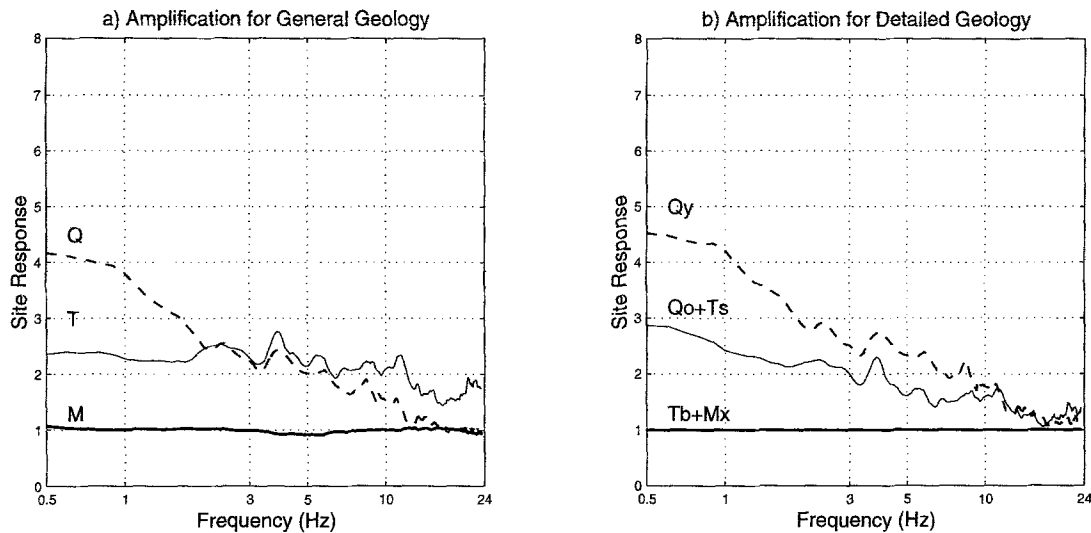


Figure 15. Average amplification for the (a) general geology and (b) detailed geology classifications. The thick line represents the site response for (a) Mesozoic and (b) Tb + Mx classes. The thin line represents the (a) Tertiary and (b) Qo + Ts classes. The dashed line represents the (a) Quaternary and (b) Qy classes. The detailed geology classification shows a better correlation between average site response and surface geology than the general geology classification.

Table 4  
Amplification Values for 1.0, 3.0, and 10.0 Hz for the Detailed and General Geology Classifications.

Freq. (Hz)	Tb + Mx		Qo + Ts		Qy		M		T		Q	
	$\bar{a}$	$\sigma$	$\bar{a}$	$\sigma$	$\bar{a}$	$\sigma$	$\bar{a}$	$\sigma$	$\bar{a}$	$\sigma$	$\bar{a}$	$\sigma$
1.00	1.00	1.06	2.42	1.34	4.22	1.14	1.01	1.08	2.27	1.41	3.80	1.17
3.00	1.00	1.30	2.00	1.72	2.51	1.21	1.00	1.41	2.28	1.58	2.23	1.24
10.0	1.00	1.14	1.59	1.73	1.77	1.12	1.01	1.18	2.09	1.33	1.54	1.19

$\bar{a}$  and  $\sigma$  represent the mean and the standard deviation of the mean, respectively. Station PAS was excluded from the Tb + Mx and M classes because it has data only up to 8.0 Hz.

of the 1994 Northridge event recorded at 31 stations of the SCEC Portable Deployment, TERRAscope, and Southern California Seismic Networks.

The direct spectral ratios determined from the 10-sec window of the *S* wave and 40-sec window of the whole record are similar without any *Q* correction. However, the results from the direct spectral ratios and from the inversion scheme show that the effect of the whole path *Q<sub>s</sub>* is important, especially at high frequencies, and should be taken into account for site-response estimation when widely distributed stations are used.

The coda amplification values obtained from the vertical and horizontal components differ and depend on the chosen reference site. This dependency is diminished when the average of all rock sites is used as the reference site. When using the average of rock sites as a reference site, the coda amplification from the vertical and horizontal components are similar within a factor of 2. For stations located on rock, the coda amplification from the vertical and horizontal components produce results close to those from the inverted *S*-

wave spectra within a factor of 2. For stations in the basin, however, this factor can be greater than 2.

The receiver-function estimates, *H/V*, are capable of revealing the predominant frequency peaks; however, their amplification values are different from the amplifications determined from the *S*-wave and coda methods.

Finally, it is found that site characterizations based on a detailed geology classification distinguish more clearly the average site response than using a general geology classification only.

### Acknowledgments

We thank all those people who participated in the installation of the SCEC portable stations. We also thank SCEC for the data provided through its database. We give special thanks to Emily Heaton and Jason MacKenna who helped with the instrument calibration and Ned Field for his help and comments to improve this project. We also thank Steve Park who gave us the geology and site classification for each station. Finally, we thank Dr. Hiroshi Kawase, Dr. Mitsuyuki Hoshiba, and Dr. Feng Su for their constructive comments and corrections. This study was supported by the Ec-

uador Development Scholarship Program through the U.S. Agency for International Development, the National Science Foundation through Cooperative Agreement EAR-8920136, USGS Cooperative Agreement 14-08-0001-A0899 to the Southern California Earthquake Center (SCEC), and USGS National Earthquake Hazard Reduction Program Award 1434-94-G2410. Development of the computerized inversion code was supported by the Nuclear Regulatory Commission, NRC-04-94-079. ICS contribution paper 0242-53EQ.

## References

- Aki, K. (1993). Local site effects on weak and strong ground motion. *Tectonophysics* **218**, 93–111.
- Aki, K. and B. Chouet (1975). Origin of coda waves: source, attenuation, and scattering effects, *J. Geophys. Res.* **80**, 3322–3342.
- Borcherdt, R. D. (1970). Effects of local geology on ground motion near San Francisco Bay, *Bull. Seism. Soc. Am.* **60**, 29–61.
- Borcherdt, R. D. and J. F. Gibbs (1976). Effects of local geological conditions in the region on ground motions and intensities of the 1906 earthquakes, *Bull. Seism. Soc. Am.* **66**, 467–500.
- Chin, B. H. and K. Aki (1991). Simultaneous determination of source, path, and recording site effects on strong ground motion during the Loma Prieta earthquake: a preliminary result on pervasive nonlinear site effect, *Bull. Seism. Soc. Am.* **81**, 1859–1884.
- Edelman, A. and F. Vernon (1995). The Northridge portable instrument aftershock data set, SCEC Data Product Report, University of California, San Diego.
- Fehler, M., M. Hoshiba, H. Sato, and K. Obara (1992). Separation of scattering and intrinsic attenuation for the Kanto-Toaki region, Japan, using measurements of S-wave energy vs. hypocentral distance, *Geophys. J. Int.* **108**, 787–800.
- Field, E. H. (1996). Spectral amplification in a sediment-filled valley exhibiting clear basin-edge induced waves, *Bull. Seism. Soc. Am.* **86**, 991–1005.
- Field, E. H. and K. H. Jacob (1995). A comparison and test of various site response estimation techniques, including three that are non reference-site dependent, *Bull. Seism. Soc. Am.* **85**, 1127–1143.
- Field, E. H., K. H. Jacob, and S. E. Hough (1992). Earthquake site response estimation: a weak-motion case study, *Bull. Seism. Soc. Am.* **82**, 2283–2307.
- Frankel, A. (1993). Three-dimensional simulations of ground motions in the San Bernardino Valley, California, for hypothetical earthquakes on the San Andreas Fault, *Bull. Seism. Soc. Am.* **83**, 1020–1041.
- Gao, S., H. Liu, P. M. Davis, and L. Knopoff (1996). Localized amplification of seismic waves and correlation with damage due to the Northridge earthquake, *Bull. Seism. Soc. Am.* **86**, S209–S230.
- Hartzell, S. H. (1992). Site response estimation from earthquake data, *Bull. Seism. Soc. Am.* **82**, 2308–2327.
- Hartzell, S. H., A. Leeds, A. Frankel, and J. Michael (1996). Site response for urban Los Angeles using aftershocks of the Northridge earthquake, *Bull. Seism. Soc. Am.* **86**, S168–S192.
- Kato, K., K. Aki, and M. Takemura (1995). Site amplification from coda-waves: validation and application to S-wave site response, *Bull. Seism. Soc. Am.* **85**, 467–477.
- Koyanagi, S., K. Mayeda, and K. Aki (1992). Frequency-dependent site amplification factors using the S-wave coda for the island of Hawaii, *Bull. Seism. Soc. Am.* **82**, 1151–1185.
- Lachet, C. and P.-Y. Bard (1994). Numerical and theoretical investigations on the possibilities and limitations of Nakamura's technique, *J. Phys. Earth* **42**, 377–397.
- Lachet, D., C. Hatzfeld, P.-Y. Bard, N. Theodulis, C. Papaioannou, and A. Savvaidis (1996). Site effects and microzonation in the city of Thessaloniki (Greece), comparison of different approaches, *Bull. Seism. Soc. Am.* **86**, 1692–1703.
- Langston, C. A. (1979). Structure under Mount Rainier, Washington, inferred from teleseismic body waves, *J. Geophys. Res.* **84**, 4749–4762.
- Lermo, J. and F. J. Chávez-García (1993). Site effect evaluation using spectral ratios with only one station, *Bull. Seism. Soc. Am.* **83**, 1574–1594.
- Margheriti, L., L. Wennerberg, and J. Boatwright (1994). A comparison of coda and S-wave spectral ratio estimates of site response in the southern San Francisco Bay area, *Bull. Seism. Soc. Am.* **84**, 1815–1830.
- Mayeda, K., S. Koyanagi, and K. Aki (1991). Site amplifications from S-wave coda in the Long Valley caldera region, California, *Bull. Seism. Soc. Am.* **81**, 2194–2213.
- Menke, W. (1989). *Geophysical Data Analysis: Discrete Inverse Theory*, Academic, New York.
- Olsen, K. B. and R. J. Archuleta (1996). Three-dimensional simulation of earthquakes on the Los Angeles fault system, *Bull. Seism. Soc. Am.* **86**, 575–596.
- Park, S., S. Elrick, and E. Lehmer (1996). Extrapolation of site classification using quaternary geologic mapping in the Los Angeles region, Southern California Earthquake Center, Internal Report.
- Phillips, W. S. and K. Aki (1986). Site amplification of coda waves from local earthquakes in central California, *Bull. Seism. Soc. Am.* **76**, 627–648.
- Shoja-Taheri, J. and B. A. Bolt (1977). A generalized strong-motion accelerogram based on spectral maximization from two horizontal components, *Bull. Seism. Soc. Am.* **67**, 863–876.
- Singh, S. K. and M. Ordaz (1993). On the origin of long coda observed in the lake-bed strong-motion records of Mexico City, *Bull. Seism. Soc. Am.* **83**, 1298–1306.
- Steidl, J. H. (1993). Variation of site response at the UCSB dense array of portable accelerometers, *Earthquake Spectra* **9**, 289–302.
- Steidl, J. H., L. F. Bonilla, and A. G. Tumarkin (1995). Seismic hazard in the San Fernando basin, Los Angeles, CA: a site effects study using weak-motion and strong-motion data, *Proc. of the 5th International Conference on Seismic Zonation*, Nice, France, 1149–1156.
- Steidl, J. H., A. G. Tumarkin, and R. J. Archuleta (1996). What is a reference site?, *Bull. Seism. Soc. Am.* **86**, 1733–1748.
- Su, F. and K. Aki (1995). Site amplification factors in central and southern California determined from coda waves, *Bull. Seism. Soc. Am.* **85**, 452–466.
- Su, F., J. G. Anderson, J. N. Brune, and Y. Zeng (1996). A comparison of direct S-wave and coda wave site amplification determined from aftershocks of Little Skull Mountain earthquake, *Bull. Seism. Soc. Am.* **86**, 1006–1018.
- Tinsley, J. C. and T. E. Fumal (1985). Mapping Quaternary sedimentary deposits for areal variations in shaking response, in *Evaluating Earthquake Hazards in the Los Angeles Region*, U.S. Geol. Surv. Profess. Pap. 1360, 101–125.
- Tumarkin, A. G. and R. J. Archuleta (1992). Parametric models of spectra for ground motion prediction, *Seism. Res. Lett.* **69**, 30.
- Wald, L., L. K. Hutton, and D. D. Given (1995). The Southern California Bulletin: 1990–1993 summary, *Seism. Res. Lett.* **66**, Jan–Feb.
- Institute for Crustal Studies  
University of California at Santa Barbara  
Santa Barbara, California 93106-1100  
(L.F.B., J.H.S., G.T.L., A.G.T., R.J.A.)
- Department of Geological Sciences  
University of California at Santa Barbara  
Santa Barbara, California 93106-1100  
(L.F.B., R.J.A.)